SCIENTIFIC REPORTS

OPEN

Superconductivity at 38 K at an electrochemical interface between an ionic liquid and $FeSe_{0.8}Te_{0.2}$ on various substrates

Received: 29 May 2018
Accepted: 13 September 2018
Published online: 03 October 2018

Shunsuke Kouno[1], Yohei Sato[1], Yumiko Katayama[1], Ataru Ichinose[2], Daisuke Asami[1], Fuyuki Nabeshima[1], Yoshinori Imai[3], Atsutaka Maeda[1] & Kazunori Ueno[1]

Superconducting $FeSe_{0.8}Te_{0.2}$ thin films on $SrTiO_3$, $LaAlO_3$ and CaF_2 substrates were electrochemically etched in an ionic liquid, DEME-TFSI, electrolyte with a gate bias of 5 V. Superconductivity at 38 K was observed on all substrates after the etching of films with a thickness greater than 30 nm, despite the different T_c values of 8 K, 12 K and 19 K observed before etching on $SrTiO_3$, $LaAlO_3$ and CaF_2 substrates, respectively. T_c returned to its original value with the removal of the gate bias. The observation of T_c enhancement for these thick films indicates that the T_c enhancement is unrelated to any interfacial effects between the film and the substrate. The sheet resistance and Hall coefficient of the surface conducting layer were estimated from the gate bias dependence of the transport properties. The sheet resistances of the surface conducting layers of the films on $LaAlO_3$ and CaF_2 showed identical temperature dependence, and the Hall coefficient was found to be almost independent of temperature and to take values of −0.05 to −0.2 m^2/C, corresponding to 4–17 electrons per $FeSe_{0.8}Te_{0.2}$ unit cell area in two dimensions. These common transport properties on various substrates suggest that the superconductivity at 38 K appears in the surface conducting layer as a result of an electrochemical reaction between the surface of the $FeSe_{0.8}Te_{0.2}$ thin film and the ionic liquid electrolyte.

FeSe is an iron-based superconductor with the simplest possible composition and exhibits superconductivity at 8.5 K[1]. FeSe has recently attracted considerable attention owing to the enhancements in the superconducting transition temperature (T_c) that can be achieved through various methods. The T_c of a one-unit-cell FeSe thin film on a $SrTiO_3$ substrate has been reported to take values of 105 K and 85 K based on an *in situ* resistivity measurement and a diamagnetic measurement, respectively[2,3]. Spectroscopic studies of monolayer and several-layer FeSe on $SrTiO_3$ have revealed superconducting gaps corresponding to 65 K and 80 K by means of angle-resolved photoemission spectroscopy (ARPES) and scanning tunneling microscopy (STM), respectively[4–6]. These values are much higher than the bulk T_c values of all known iron-based superconductors. A T_c of 48 K has also been observed in several-layer FeSe on $SrTiO_3$ with carrier doping by K ions[7]. This T_c enhancement has been suggested to originate from charge transfer from the oxide substrate to the ultrathin FeSe film[6]. T_c enhancements of up to approximately 40 K have also been reported following the insertion of cations or a $(Li_{0.8}Fe_{0.2})OH$ layer to the FeSe mother compound[8–14]. Recently, electrostatic carrier doping on ultrathin FeSe films and flakes has also been found to enhance T_c up to approximately 40 K[15–19]. The authors of these studies employed an electric double layer transistor (EDLT) configuration with an ionic liquid, diethylmethyl(2-methoxyethyl)ammonium bis(trifluoromethylsulfonyl)imide (DEME-TFSI), as a gate electrolyte for tuning the high-density carriers[20–22]. Since no additional phase other than FeSe was found in the X-ray diffraction (XRD) data[18], the T_c enhancement was concluded to originate from electrostatic carrier doping. In addition, a thickness dependence study conducted by means of the electrochemical etching of FeSe showed that T_c enhancement occurred only when the film was thinner than 15 nm[16,19], probably indicating that the interface between the film and the substrate also plays an important role in the T_c enhancement.

[1]Department of Basic Science, University of Tokyo, Meguro, Tokyo, 153-8902, Japan. [2]Central Research Institute of Electric Power Industry, Yokosuka, Kanagawa, 240-0196, Japan. [3]Department of Physics, Tohoku University, Sendai, 980-8578, Japan. Correspondence and requests for materials should be addressed to K.U. (email: ueno@phys.c.u-tokyo.ac.jp)

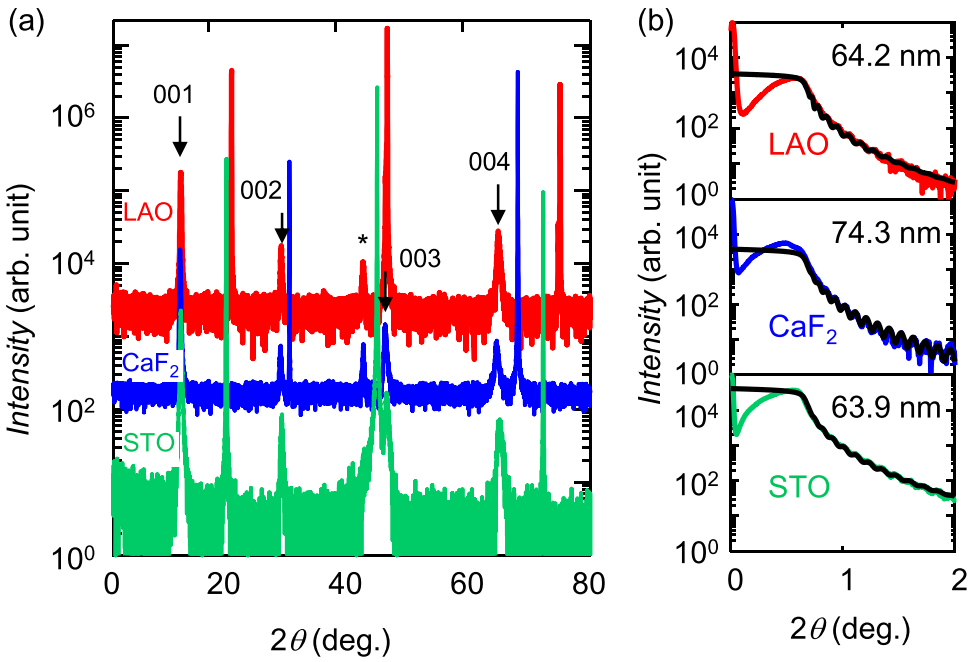

Figure 1. (**a**) X-ray diffraction (XRD) patterns of $FeSe_{0.8}Te_{0.2}$ thin films on $LaAlO_3$ (LAO), CaF_2 and $SrTiO_3$ (STO) substrates. (**b**) X-ray reflectivity (XRR) patterns of the films. The black lines represent fit curves. The estimated thickness is shown in each panel.

We have previously reported T_c enhancements in $FeSe_{1-x}Te_x$ thin films on various substrates[23–26]. The observed T_c values depend on both the Te content and the substrate material. For example, the T_c values for $FeSe_{0.8}Te_{0.2}$ films on CaF_2 and $LaAlO_3$ substrates are enhanced to 20 K and 12 K, respectively, in contrast to the T_c of 8 K observed for $FeSe_{0.8}Te_{0.2}$ on $SrTiO_3$. This can be explained by differences in the a-axis lattice constants of $FeSe_{0.8}Te_{0.2}$ films on different substrates[24]. In this paper, we report the enhancement of T_c up to 38 K for thick $FeSe_{0.8}Te_{0.2}$ films on various substrates prepared via EDLT fabrication with the ionic liquid DEME-TFSI. By means of electrochemical etching with the ionic liquid[16], the film thickness was varied. The application of a gate bias resulted in the formation of a surface conducting layer with a T_c of 38 K; with the removal of the gate bias, the surface conducting layer disappeared, causing T_c to return to its original value. We also estimated the transport properties of the surface conducting layer. The surface conducting layer exhibited electron conduction with a common dependence of the mobility on temperature on various substrates.

Results

Characterization of $FeSe_{0.8}Te_{0.2}$ thin films. The film thickness and crystal quality were examined via XRD measurements. Figure 1(a) shows the XRD patterns of $FeSe_{0.8}Te_{0.2}$ thin films fabricated on $LaAlO_3$ (LAO), CaF_2 and $SrTiO_3$ (STO) substrates. All samples exhibited (001), (002) and (004) peaks, while the (003) peak for the film on the LAO substrate was obscured by a (002) peak of the substrate. The c-axis lattice constants for the films on the LAO, CaF_2 and STO substrates were 5.69, 5.72 and 5.70 A, respectively, consistent with previous reports[23,24]. The full widths at half maximum (FWHMs) of the rocking curves for the (001) peak were 0.4, 0.7 and 1 deg. for the films on the LAO, CaF_2 and STO substrates, respectively; these values are also almost the same as those reported previously (0.2–0.6 deg.)[23], demonstrating that all of these films consisted of high-quality single-phase samples. X-ray reflectivity (XRR) measurements revealed clear thickness fringes for all films, as shown in Fig. 1(b), indicating a smooth surface and a sharp interface between the film and the substrate. In addition, all XRR curves were well fitted by the model structure, and we estimated the thicknesses as shown in Fig. 1(b). The film thicknesses were also confirmed by atomic force microscopy (AFM) images of the films.

Superconducting properties of pristine and etched $FeSe_{0.8}Te_{0.2}$ thin films. The superconducting properties of the samples when subjected to gating and etching were examined for a gate bias (V_G) of 5 V. As shown in Fig. 2(a), the EDLT samples were patterned in Hall bars with six electrodes, and a Pt film was placed alongside each Hall-bar-instrumented sample to act as a gate electrode. Figure 2(c,d) show the temperature (T) dependences of the sheet resistance (R_S) for samples of $FeSe_{0.8}Te_{0.2}$ films on LAO and CaF_2 substrates (LAO and CaF_2 samples), respectively. First, the R_S-T curves of the pristine sample before etching were measured for V_G values of of 0 V and 5 V. Then, the temperature was increased to 250 K with a V_G of 5 V while monitoring the gate current (I_G), as shown in Fig. 2(b). The channel was electrochemically etched, and the drain current (I_D) was gradually decreased. The product of I_G and time is a Faradaic charge (Q_F) that is proportional to the amount of charge of the reacted ions. After etching, T was decreased while maintaining $V_G = 5$ V, and the R_S–T curve was measured. After several cycles of etching, the V_G dependence of the R_S–T curve for the etched sample was measured via the following procedure: First, the R_S–T curve was measured for a V_G of 5 V. Then, the temperature

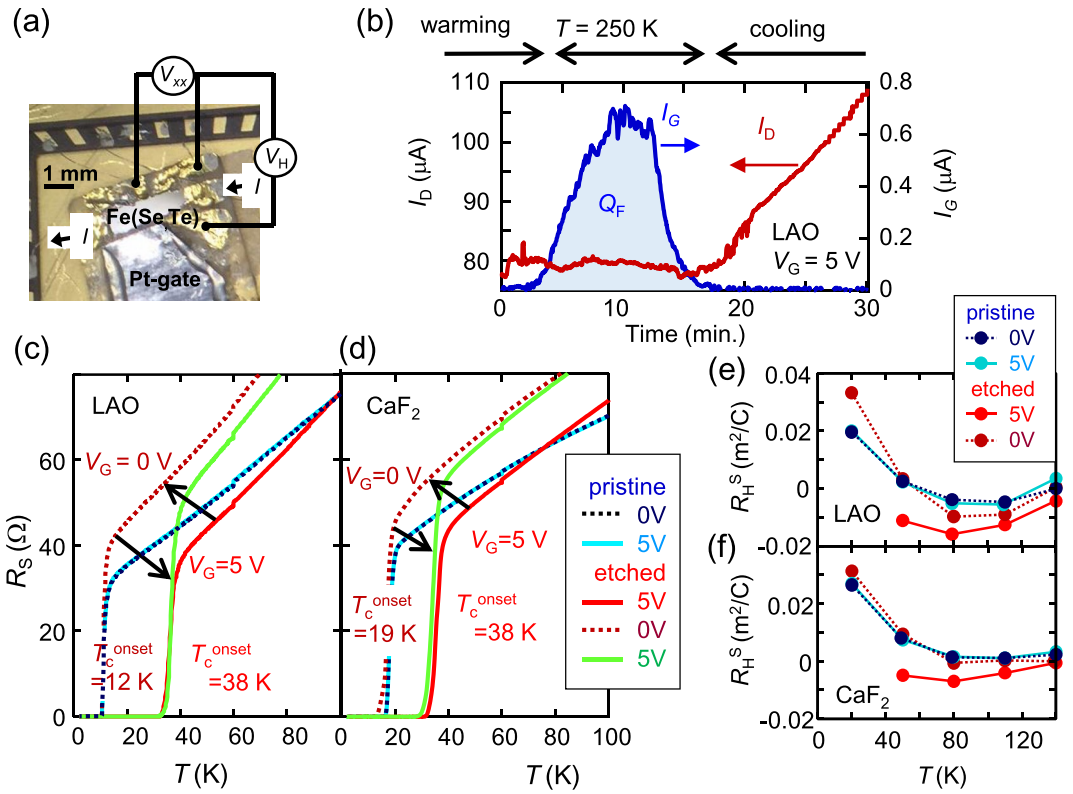

Figure 2. Changes in the superconducting and transport properties of $FeSe_{0.8}Te_{0.2}$ samples subjected to electrochemical etching and gating. (**a**) A photographic image of the electric double layer transistor (EDLT) device on the $FeSe_{0.8}Te_{0.2}$/LAO sample. The four-terminal resistance and the Hall resistance were simultaneously measured with the Hall bar electrodes. The ionic liquid electrolyte was placed between the film and the Pt gate. (**b**) The time dependences of the drain current (I_D) and the gate current (I_G) during electrochemical etching at $V_G = 5$ V and 250 K for the $FeSe_{0.8}Te_{0.2}$/LAO sample. I_G corresponds to the Faradaic current, and the product of I_G and time corresponds to the Faradaic charge (Q_F). (**c**,**d**) The temperature (T) dependences of the sheet resistance (R_S) for the $FeSe_{0.8}Te_{0.2}$ samples fabricated on the LAO and CaF_2 substrates, respectively. Each panel shows the R_S-T curves with and without gating for the pristine and etched samples. For each etched sample, bias voltages V_G of 5 V (red solid line), 0 V (red broken line), and 5 V (purple solid line) were applied in that order. For each pristine sample, bias voltages V_G of 0 V (blue broken line) and 5 V (blue solid line) were applied in that order. (**e**,**f**) The T dependences of the Hall coefficient (R_H) for the samples on the LAO and CaF_2 substrates, respectively. Each panel shows the R_H-T curves with and without gating for the pristine and etched samples.

was increased to 250 K without V_G, and the R_S–T curve for $V_G = 0$ V was measured. Finally, a V_G of 5 V was again applied at 250 K, and the R_S–T curve for $V_G = 5$ V was measured again. We show the R-T curves of the pristine and etched samples for $V_G = 5$ V, $V_G = 0$ V, and $V_G = 5$ V. The R_S–T curves of the pristine samples remained almost unchanged between the V_G values of 0 V and 5 V. In contrast, T_c was enhanced after several cycles of etching at $V_G = 5$ V. T_c increased from 12 K to 38 K for the LAO sample and from 19 K to 38 K for the CaF_2 sample. As shown in S. Fig. 3 in the Supplementary Information, critical magnetic field at 0 K was also enhanced from 47 T to 67 T on films on the LAO substrate. The coherence length at 0 K was 3.8 nm to 3.1 nm. With the removal of V_G, R_S increased, and T_c returned to the value of the pristine sample. With the application of a V_G of 5 V, R_S slightly decreased, and T_c was enhanced to 38 K for both samples. Notably, the R_S value at $V_G = 5$ V after the removal of the initial V_G was larger than that before the removal of V_G. Since the sheet resistance due to electrostatic carrier doping should always have the same value at $V_G = 5$ V, this difference suggests that the change in R_S can be attributed to some other origin than electrostatic carrier doping. In addition, the T_c for $V_G = 0$ V was different for the LAO and CaF_2 sample because of different lattice constant of the $FeSe_{0.8}Te_{0.2}$ films. If the surface conducting layer is produced by an electrostatic carrier doping, it is natural that the surface conducting layer also show different T_c values for $V_G = 5$ V. Then, the T_c enhancement to 38 K for both samples also suggests that the origin of the carrier doping is not the electrostatic doping. This will be discussed later. Figure 2(e,f) show the T dependences of the Hall coefficient (R_H) for the same samples shown in Fig. 2(c,d), respectively. R_H was almost zero above 80 K and showed an increase with decreasing temperature below 40 K for the pristine samples. In contrast, R_H was always negative at all temperatures for the etched samples at $V_G = 5$ V. The R_H-T behavior returned to almost the original one after the application of $V_G = 0$ V. These results indicate that the etching at $V_G = 5$ V resulted in the formation of a conducting layer on the surface, with a T_c of 38 K, for both the LAO and CaF_2 samples. Since R_H was negative, electron conduction dominated in the conductive layer. In addition, since the transport properties of the pristine

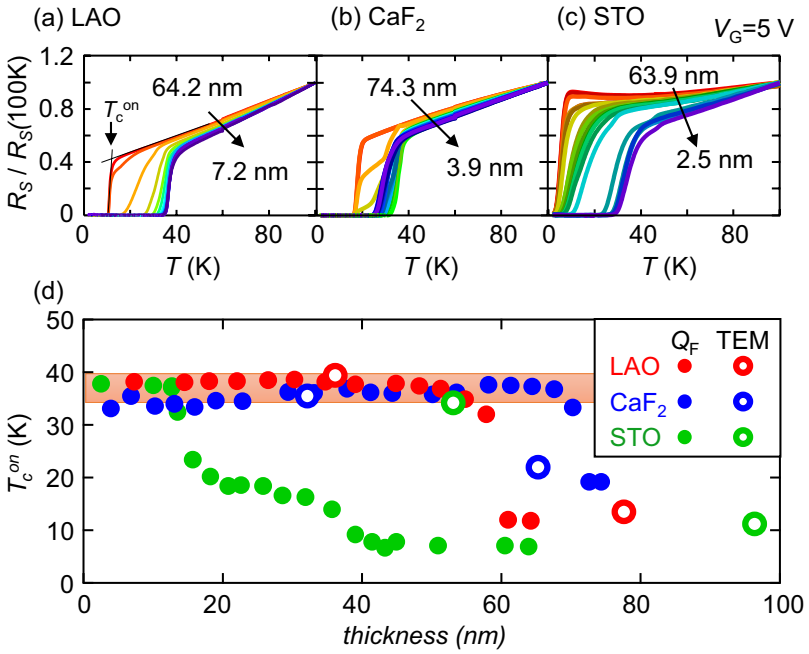

Figure 3. Variations in the superconducting transition temperature with changes in thickness for $FeSe_{0.8}Te_{0.2}$ samples on various substrates. (**a**–**c**) The T dependences of R_S (normalized to the R_S value at 100 K, R_S(100 K)) for LAO, CaF_2 and STO samples, respectively, subjected to electrochemical etching at $V_G = 5$ V. (**d**) The thickness dependences of T_c^{onset} for the three samples. Filled symbols correspond to the data shown in (**a**–**c**), for which the thickness was estimated from Q_F. Open symbols correspond to other samples whose thicknesses after etching were directly measured via TEM, as shown in Fig. 4.

and etched samples were almost the same for a V_G of 0 V, it can be concluded that the surface conductive layer disappeared with the removal of V_G from the etched sample.

Thickness dependence of the superconducting properties of $FeSe_{0.8}Te_{0.2}$ thin films. The thickness dependence of the superconducting properties was also examined for the LAO, CaF_2 and STO samples. Figure 3(a–c) show the R_S-T curves of the LAO, CaF_2 and STO samples, respectively, with various thicknesses (numbers of etching cycles). R_S is normalized to the R_S value at 100 K. For the LAO and CaF_2 samples, T_c was enhanced after several cycles of etching. The CaF_2 sample showed a two-step superconducting transition during the initial stage of etching. A similar two-step transition has been reported for an EDLT configuration on an FeSe flake with a gate bias of approximately 4 V and has been ascribed to the inhomogeneity of the carrier distribution[15]. In addition, the normalized R_S-T curves after the T_c enhancement were nearly identical. In contrast, for the STO sample, T_c was gradually enhanced from 8 K to 38 K over many cycles. We estimated the onset temperature (T_c^{onset}) of superconductivity from the R_S-T curve as shown in Fig. 3(a). We also estimated the thickness after n cycles of etching, *thickness(n)*, from the following equation:

$$thickness(n) = thickness(XRR) \times \sum_{i=1}^{n} Q_F / \sum_{i=1}^{n\_total} Q_F,$$

where Q_F is the Faradaic charge for each cycle, *thickness(XRR)* is the film thickness before etching as estimated from the XRR measurement, and n_{total} is the total number of cycles needed for the etching of the entire film. After the total etching of the film, the sample resistance is larger than MOhm. In addition, the film totally disappeared after the etching experiment. Therefore, we assumed the entire film was etched during the n_{total} cycles of etching. Figure 3(d) shows the thickness dependence of T_c^{onset} for the LAO, CaF_2 and STO samples. T_c started to increase only after two cycles of etching and saturated at 38 K after four cycles for the LAO and CaF_2 samples. As reported in the previous paragraph, T_c decreased to its original value with the removal of V_G at 250 K, but it returned to 38 K after the next application of $V_G = 5$ V for the next cycle. The STO sample showed T_c enhancement from 8 K to 16 K at a thickness of 30 nm and a further T_c enhancement to 38 K at a thickness of 10 nm. Since T_c enhancement was observed for thick samples on all substrates, and since T_c changed with the application and removal of V_G, we conclude that this T_c enhancement was not affected by the interface between the substrate and the film but instead originated from the surface conducting layer produced by $V_G = 5$ V.

The thickness of the samples which showed the T_c enhancement was confirmed by means of transmission electron microscopy (TEM) and XRD measurements. We performed corresponding etching experiments using other samples on LAO, CaF_2 and STO substrates and terminated the etching process after several cycles. All of the etched samples showed superconductivity at T_c values above 34 K. The film thickness after etching was directly obtained via TEM measurements. The thickness dependences of T_c^{onset} for these samples are shown in

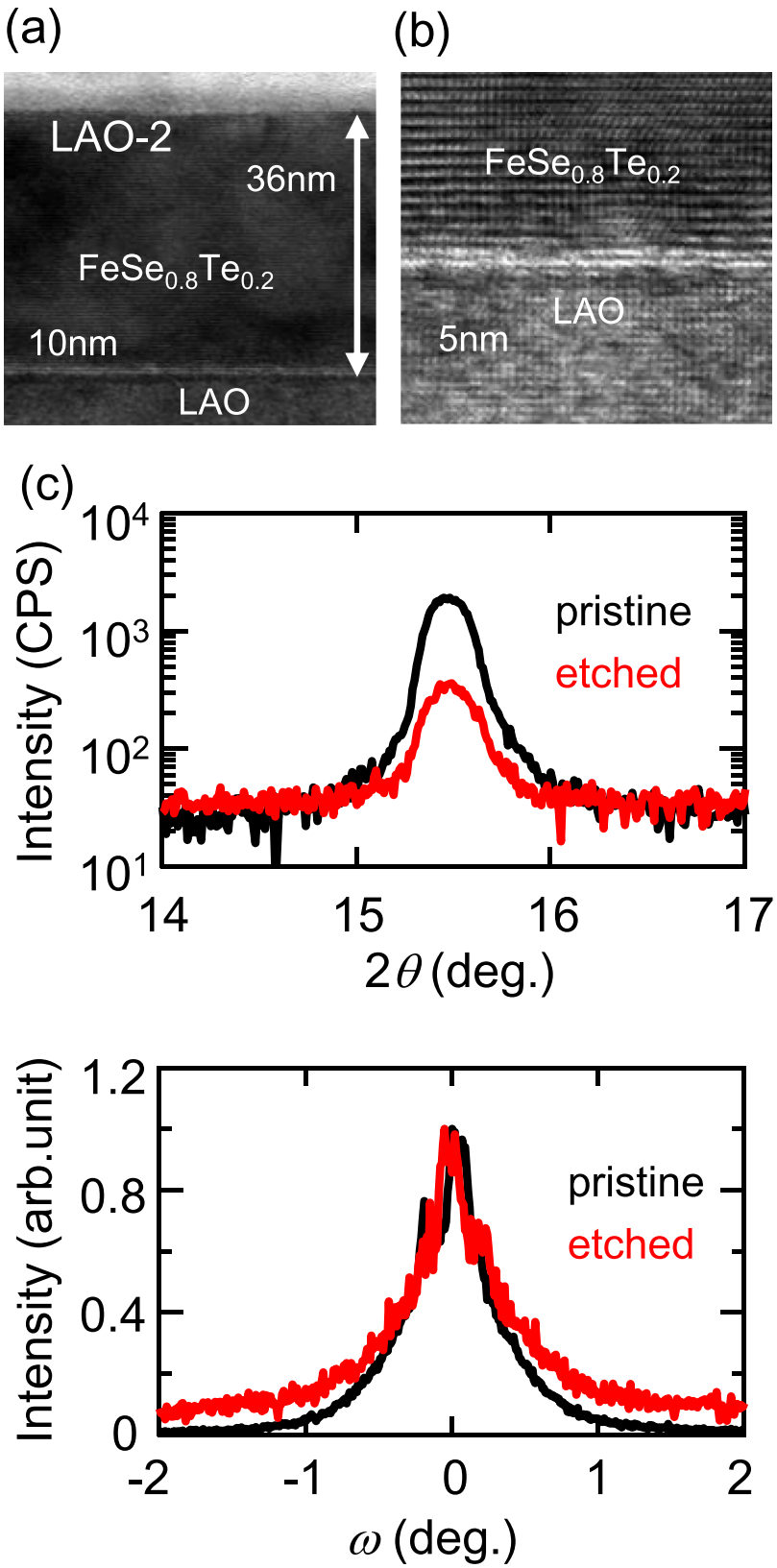

Figure 4. TEM and XRD data for the same sample on a LAO substrate before (pristine) and after (etched) electrochemical etching. (**a**,**b**) TEM images of the etched sample. (**c**,**d**) XRD patterns and rocking curves, respectively, for the (001) diffraction peak of the $FeSe_{0.8}Te_{0.2}$ film. The intensity is normalized to the intensity at $\omega = 0$.

Fig. 3(d). The $FeSe_{0.8}Te_{0.2}$ films on LAO, CaF_2 and STO substrates all showed T_c enhancement for films with thicknesses greater than 30 nm. As shown in Fig. 4(a,b) and in S. Fig. 1(a,e) in the Supplementary Information, the interface between the substrate and the film was smooth for all films, and a clear periodicity of the atomic arrays was observed. The bright region at the interface probably indicates Se diffusion from the film into the substrate[27,28]. For the film on the LAO substrate, the clear periodicity remained at the surface, and no additional layer was found on the film, as shown in Fig. 4(a). On the CaF_2 and STO substrates, a disordered FeO_x layer was found on the ordered region with clear periodicity. The T_c enhancement probably occurred in this ordered region. XRD patterns recorded before and after etching indicated that the peak position remained unchanged and that no new peak was present after etching, as shown in Fig. 4(c); the only observed difference was a decrease in the peak intensity. In addition, the FWHM of the rocking curve for the (001) peak remained unchanged, as shown in Fig. 4(d). These XRD data indicated that no new phase was created in the film by the etching process. Thus, no electrochemical reaction occurred in the bulk of the film; instead, such reactions took place only at the surface.

We also examined the thickness dependence of T_c for FeSe films on LAO and STO substrates. As shown in S. Fig. 2(a,b), these films showed T_c enhancements of up to 30 or 40 K upon etching. On STO substrates, only films with thicknesses below 12 nm showed T_c enhancement. This finding coincides with those of previous reports[16]. In contrast, a film with a thickness of 30 nm on the LAO substrate showed T_c enhancement, similar to the behavior of $FeSe_{0.8}Te_{0.2}$ films. Notably, several $FeSe_{0.8}Te_{0.2}$ samples on CaF_2 and STO substrates showed T_c enhancement to above 37 K only for thicknesses below 10 nm. The different critical thicknesses for FeSe and $FeSe_{0.8}Te_{0.2}$ films on different substrates were probably due to differences in the homogeneity of the films. As shown in S. Fig. 1(a,e) in the Supplementary Information, a disordered region was observed in the $FeSe_{0.8}Te_{0.2}$ film on STO. In addition, a disordered Fe (or FeO_x) layer was observed on top of the $FeSe_{0.8}Te_{0.2}$ films on CaF_2 and STO substrates. These TEM images indicate that the film quality depends on the substrate and that the best quality is achieved for $FeSe_{0.8}Te_{0.2}$ films on LAO substrates. We consider that good film quality throughout the entire film is necessary for the occurrence of T_c enhancement for a thick film. Thus, although we did not perform TEM measurements of all of these samples, the lack of T_c enhancement to 38 K for the thick films on some samples might have been due to insufficient film homogeneity, especially near the surface.

Discussion

Finally, we discuss the origin of the T_c enhancement. The T_c enhancement has been reported to be due to charge accumulation on the surface of the FeSe[15,16,18]. However, an electrochemically reacted layer on the surface may also show a high T_c, since FeSe samples intercalated with alkali ions and/or organic molecules present T_c values above 40 K[8,9]. To distinguish electrostatic charge accumulation from electrochemical reaction, we estimated the sheet resistance and Hall coefficient of the surface layer. The resistance tensor, ρ, and the conductance tensor, σ, are represented by the following equations:

$$\rho = \begin{pmatrix} R_S & -R_H B \\ R_H B & R_S \end{pmatrix} \tag{1}$$

$$\sigma = \rho^{-1} = \frac{1}{R_S^2 + R_H^2 B^2}\begin{pmatrix} R_S & R_H B \\ -R_H B & R_S \end{pmatrix} \sim \begin{pmatrix} \frac{1}{R_S} & \frac{R_H B}{R_S} \\ -\frac{R_H B}{R_S} & \frac{1}{R_S} \end{pmatrix} \tag{2}$$

where B is the magnetic field applied during the Hall measurement. The σ of a sample at $V_G = 5$ V is equal to the sum of the σ values of the sample at $V_G = 0$ V and of the surface conducting layer produced by a V_G of 5 V. Therefore, the sheet resistance and Hall coefficient of the surface conducting layer, $R_S^{surface}$ and $R_H^{surface}$, obey the following equations:

$$\frac{1}{R_{xx}(V_G = 5V)} = \frac{1}{R_{xx}(V_G = 0V)} + \frac{1}{R_{xx}^{surface}} \tag{3}$$

$$\frac{R_H(V_G = 5V)}{R_{xx}(V_G = 5V)} = \frac{R_H(V_G = 0V)}{R_{xx}(V_G = 0V)} + \frac{R_H^{surface}}{R_{xx}^{surface}} \tag{4}$$

As shown in Fig. 5(b–d), we examined the changes in the sheet resistance and Hall coefficient for one V_G cycle of a LAO sample (LAO-1, as shown in Fig. 2(c)) and two V_G cycles of a CaF_2 sample (CaF_2-1 and CaF_2-2, where the data for CaF_2-1 are shown in Fig. 2(d)). Figure 5(a) shows the temperature dependence of $R_S^{surface}$ normalized to the value at 90 K. The R_S-T curves for the LAO and CaF_2 samples just before the last etching cycle, R_S(last), are also plotted. All curves follow almost the same profile. This indicates that the transport properties, such as the electron mobility and scattering time, of all samples exhibited identical temperature dependences. As shown in the inset of Fig. 5(a), R_H was almost independent of temperature and negative for all samples. Electron-type conduction is a common feature in previous reports on the T_c enhancement of FeSe[7,15–18], and the vanishing of the hole pocket at the Fermi level has been considered to be the origin of the T_c enhancement[7,15,16]. The observed Hall coefficient values of 0.05 to 0.2 m^2/C correspond to 4–17 electrons per unit cell in two dimensions (0.376 nm × 0.376 nm). If such a high density of carriers were electrostatically accumulated on the surface, then electrons would be strongly scattered at the surface, and the scattering time should change with the variation

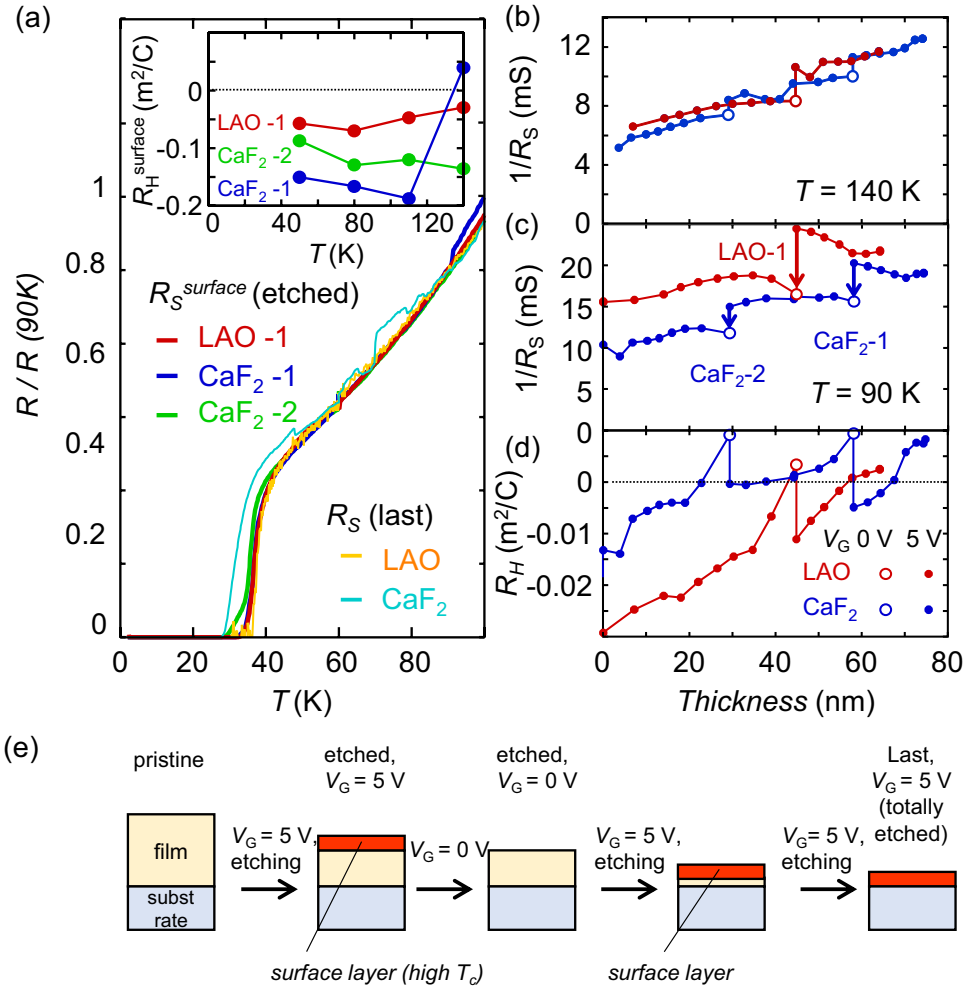

Figure 5. Superconducting transition for the surface conducting layer and changes in the transport properties with electrochemical etching for various samples. (**a**) The T dependence of the R_S values of the surface conducting layer ($R_S^{surface}$), normalized to the value at 90 K. $R_S^{surface}$ was estimated from the change in the sheet conductance between V_G values of 5 V and 0 V. Data for three V_G cycles of two samples, labeled as LAO-1, CaF_2-1 and CaF_2-2 in (**c**), are shown. The R_S-T curves just before the last etching cycle for the LAO and CaF_2 samples are also plotted. The inset shows the R_H values of the surface conducting layers of the LAO-1, CaF_2-1 and CaF_2-2 samples as a function of temperature. (**b**–**d**) Values of $1/R_S$ at 140 K and 50 K and of R_H at 50 K, respectively, as functions of the film thickness for the LAO and CaF_2 samples. V_G was changed from 5 V to 0 V once and twice during the etching of the LAO and CaF_2 samples, respectively. (**e**) Schematic illustration of the evolution of a sample during etching. A surface layer is formed during etching and disappears with the removal of the gate bias.

in the accumulated carrier density[29]. However, no such change was observed in the R-T curves. In addition, as shown previously in Fig. 2(c,d), the removal of V_G irreversibly changed R_S, suggesting that the origin of the change in R_S is some other phenomenon than electrostatic carrier doping. Therefore, a different cause of carrier doping other than the electric field effect is likely responsible for the T_c enhancement.

Both the irreversible change in R_S with V_G and the lack of variation in the electron mobility with the carrier doping can be explained by assuming that the surface conducting layer is formed not by the accumulation of electrostatic charge but by an electrochemical reaction between the $FeSe_{0.8}Te_{0.2}$ and the ionic liquid. We hypothesize that the etching of the film and the formation of the surface conducting layer occurred simultaneously with the application of the V_G of 5 V. One potential candidate of the forming reaction of the surface conducting layer is an electrochemical intercalation of $DEME^+$ ion,

$$FeSe_{0.8}Te_{0.2} + DEME^+ + e^- + \rightarrow FeSe_{0.8}Te_{0.2}(DEME).$$

Since observed Q_F during the reaction was much larger than Q_F needed for this reaction, other electrochemical reaction, such as electrochemical decomposition of DEME-TFSI and dissolution of $FeSe_{0.8}Te_{0.2}$, also occurs. We discussed on the possible electrochemical reactions in the Supplementary Information. In addition, we hypothesize that when this V_G was removed, the surface conducting layer disappeared, probably due to decomposition

or peeling off from the surface. Then, the abrupt decrease in the sheet conductance occurred with the removal of V_G. In addition, both the electron mobility and the volume charge carrier density should be identical among LAO-1, CaF_2-1 and CaF_2-2. This hypothesis was also supported by the change in the sheet conductance with the repeated etching of the LAO and CaF_2 samples, as shown in Fig. 5(d). The sheet conductance at 50 K decreased with the removal of V_G and, with repeated etching, gradually increased after this reduction. This behavior can be explained by an increase in the thickness of the surface conducting layer with repeated etching. If the conductance of the surface conducting layer is higher than that of the bulk $FeSe_{0.8}Te_{0.2}$ film at 50 K, then repeated etching will increase the sheet conductance at low temperatures. As the number of etching cycles increases, the ratio of the thickness of the surface conducting layer to the total film thickness will increase. Then, just before the film is totally removed, the surface conducting layer will cover almost the entire film. Consistent with this picture, the temperature dependences of the sheet resistance just before the last etching cycle for both the LAO and CaF_2 samples were also identical to that for the surface conducting layer, as shown in Fig. 5(a). We also examined two dimensionality of the superconductivity on the surface conducting layer. When the superconducting layer is thinner than the superconducting coherence length, it behaves as a two dimensional superconductor. However, as shown in S. Fig. 4 in the Supplementary Information, the surface conducting layer did not behave as a two dimensional superconductor. This suggests that superconducting layer is electrochemically formed and relatively thick.

Conclusion

In conclusion, a surface conducting layer with a T_c of 38 K was formed with the electrochemical etching of $FeSe_{0.8}Te_{0.2}$ thin films on LAO, CaF_2 and STO substrates. Since the thicknesses of all etched samples with T_c values of 38 K were greater than 30 nm, the enhancement of T_c cannot be related to any interaction between the film and the substrate. In addition, T_c enhancement was also observed for an FeSe thin film on a LAO substrate with a thickness of approximately 30 nm. The surface conducting layer again showed almost identical temperature dependences between the sheet resistance and the Hall coefficient. This finding suggests that the surface conducting layer is formed not by the accumulation of electrostatic charge on the $FeSe_{0.8}Te_{0.2}$ surface but by an electrochemical reaction between the $FeSe_{0.8}Te_{0.2}$ and the ionic liquid electrolyte. Hall coefficient measurements showed that the surface conducting layer contained 4–17 electrons per unit cell in two dimensions, with an overall negative charge. From TEM measurements, we could observe a smooth interface between the substrate and the film and a clear periodicity of the atomic arrays in the etched $FeSe_{0.8}Te_{0.2}$ film on the LAO substrate. These observations indicate that the formation of the surface conducting layer did not affect the bulk region of the film, and the surface conducting layer completely disappeared with the removal of V_G. We consider that previous studies on carrier doping in ultrathin FeSe film can be classified into two groups: those that show a T_c of approximately 40 K for a several-layer FeSe film and those that show a T_c above 65 K for a monolayer FeSe on STO. Our results indicate that the electrochemical doping of FeSe and $FeSe_{0.8}Te_{0.2}$ can result in the formation of a superconducting layer with a T_c of approximately 40 K and that no interfacial interaction is necessary for the enhancement of T_c to 40 K. However, we think that the interface between FeSe and STO is probably essential for the enhancement of T_c above 65 K. We believe that it will be possible to prepare monolayer FeSe with a T_c above 65 K with further study of the electrochemical etching of FeSe.

Methods

FeSe and $FeSe_{0.8}Te_{0.2}$ thin films were deposited by means of pulsed laser deposition (PLD) with a KrF eximer laser and an FeSe or $FeSe_{0.8}Te_{0.2}$ polycrystalline target. The fabrication conditions are described in detail elsewhere[30,31]. We used a commercially available STO (001) substrate with a step-and-terrace surface, a LAO (001) substrate and a CaF_2 (001) substrate. AFM and XRD measurements were carried out prior to device fabrication. Au(100 nm)/Ti (20 nm) films were formed via electron-beam evaporation at a base pressure of 10^{-5} Torr. Since $FeSe_{0.8}Te_{0.2}$ thin films can be damaged by exposure to high temperatures (above 100 deg. Celsius) and water during the standard processes of photolithography and dry etching, we employed a sandblasting technique at room temperature for the fabrication of Hall bar electrodes. The films were coated with a dry film resist patterned via photolithography and were etched by sandblasting with alumina emery (#220). The Hall bar electrodes and wires were coated with a silicone sealant to prevent electrochemical reactions between the electrolyte and the Au/Ti electrode. The ionic liquid DEME-TFSI was dropped onto the channel area of the Hall bar configuration and the Pt film. Electrochemical etching and transport measurements were carried out in a He atmosphere with a Quantum Design Physical Property Measurement System (PPMS) at temperatures from 300 K to 2 K.

References

1. Hsu, F.-C. *et al.* Superconductivity in the PbO-type structure α-FeSe. *Proc. Natl. Acad. Sci.* **105**, 14262–14264 (2008).
2. Ge, J.-F. *et al.* Superconductivity above 100 K in single-layer FeSe films on doped $SrTiO_3$. *Nat. Mater.* **14**, 285–289 (2015).
3. Sun, Y. *et al.* High temperature superconducting FeSe films on $SrTiO_3$ substrates. *Sci. Rep.* **4**, 6040 (2014).
4. He, S. *et al.* Phase diagram and electronic indication of high-temperature superconductivity at 65 K in single-layer FeSe films. *Nat. Mater.* **12**, 605–610 (2013).
5. Qing-Yan, W. *et al.* Interface-Induced High-Temperature Superconductivity in Single Unit-Cell FeSe Films on $SrTiO_3$. *Chin. Phys. Lett.* **29**, 037402 (2012).
6. Tan, S. *et al.* Interface-induced superconductivity and strain-dependent spin density waves in FeSe/$SrTiO_3$ thin films. *Nat. Mater.* **12**, 634–640 (2013).
7. Miyata, Y., Nakayama, K., Sugawara, K., Sato, T. & Takahashi, T. High-temperature superconductivity in potassium-coated multilayer FeSe thin films. *Nat. Mater.* **14**, 775–779 (2015).
8. Burrard-Lucas, M. *et al.* Enhancement of the superconducting transition temperature of FeSe by intercalation of a molecular spacer layer. *Nat. Mater.* **12**, 15–19 (2013).
9. Hatakeda, T. *et al.* New Alkali-Metal- and 2-Phenethylamine-Intercalated Superconductors $A_x(C_8H_{11}N)_yFe_{1-z}Se$ (A = Li, Na) with the Largest Interlayer Spacings and $T_c \sim 40$ K. *J. Phys. Soc. Jpn.* **85**, 103702 (2016).
10. Wang, A. F. *et al.* Superconductivity at 32 K in single-crystalline $Rb_xFe_{2-y}Se_2$. *Phys. Rev. B* **83**, 060512 (2011).

11. Zhang, Y. *et al*. Nodeless superconducting gap in $A_xFe_2Se_2$ (A = K, Cs) revealed by angle-resolved photoemission spectroscopy. *Nat. Mater.* **10**, 273–277 (2011).
12. Ying, T. P. *et al*. Observation of superconductivity at 30~46K in $A_xFe_2Se_2$ (A = Li, Na, Ba, Sr, Ca, Yb, and Eu). *Sci. Rep.* **2**, 426 (2012).
13. Krzton-Maziopa, A. *et al*. Synthesis of a new alkali metal–organic solvent intercalated iron selenide superconductor with T c ≈ 45 K. *J. Phys. Condens. Matter* **24**, 382202 (2012).
14. Lu, X. F. *et al*. Coexistence of superconductivity and antiferromagnetism in $(Li_{0.8}Fe_{0.2})$OHFeSe. *Nat. Mater.* **14**, 325–329 (2015).
15. Lei, B. *et al*. Evolution of High-Temperature Superconductivity from a Low-T_c Phase Tuned by Carrier Concentration in FeSe Thin Flakes. *Phys. Rev. Lett.* **116**, 077002 (2016).
16. Shiogai, J., Ito, Y., Mitsuhashi, T., Nojima, T. & Tsukazaki, A. Electric-field-induced superconductivity in electrochemically etched ultrathin FeSe films on SrTiO**3** and MgO. *Nat. Phys.* **12**, 42–46 (2016).
17. Hanzawa, K., Sato, H., Hiramatsu, H., Kamiya, T. & Hosono, H. Key Factors for Insulator -Superconductor Transition in FeSe Thin Films by Electric Field. *IEEE Trans. Appl. Supercond.* **27**, 1–5 (2017).
18. Hanzawa, K., Sato, H., Hiramatsu, H., Kamiya, T. & Hosono, H. Electric field-induced superconducting transition of insulating FeSe thin film at 35 K. *Proc. Natl. Acad. Sci.* **113**, 3986–3990 (2016).
19. Shiogai, J., Miyakawa, T., Ito, Y., Nojima, T. & Tsukazaki, A. Unified trend of superconducting transition temperature versus Hall coefficient for ultrathin FeSe films prepared on different oxide substrates. *Phys. Rev. B* **95**, 115101 (2017).
20. Ueno, K. *et al*. Electric-field-induced superconductivity in an insulator. *Nat Mater* **7**, 855–858 (2008).
21. Yuan, H. *et al*. High-Density Carrier Accumulation in ZnO Field-Effect Transistors Gated by Electric Double Layers of Ionic Liquids. *Adv. Funct. Mater.* **19**, 1046–1053 (2009).
22. Ueno, K. *et al*. Field-Induced Superconductivity in Electric Double Layer Transistors. *J. Phys. Soc. Jpn.* **83**, 032001 (2014).
23. Imai, Y., Sawada, Y., Nabeshima, F. & Maeda, A. Suppression of phase separation and giant enhancement of superconducting transition temperature in FeSe1−xTex thin films. *Proc. Natl. Acad. Sci. USA* **112**, 1937–1940 (2015).
24. Imai, Y. *et al*. Control of structural transition in $FeSe_{1-x}Te_x$ thin films by changing substrate materials. *Sci. Rep.* **7**, 46653 (2017).
25. Tsukada, I. *et al*. Epitaxial Growth of $FeSe_{0.5}Te_{0.5}$ Thin Films on CaF2 Substrates with High Critical Current Density. *Appl. Phys. Express* **4**, 053101 (2011).
26. Nabeshima, F., Imai, Y., Hanawa, M., Tsukada, I. & Maeda, A. Enhancement of the superconducting transition temperature in FeSe epitaxial thin films by anisotropic compression. *Appl. Phys. Lett.* **103**, 172602 (2013).
27. Ichinose, A. *et al*. Microscopic analysis of the chemical reaction between Fe(Te, Se) thin films and underlying CaF_2. *Supercond. Sci. Technol.* **26**, 075002 (2013).
28. Tsukada, I., Ichinose, A., Nabeshima, F., Imai, Y. & Maeda, A. Origin of lattice compression of $FeSe_{1-x}Te_x$ thin films on CaF_2 substrates. *AIP Adv.* **6**, 095314 (2016).
29. Sato, Y., Doi, K., Katayama, Y. & Ueno, K. Electrolyte dependence of transport properties of $SrTiO_3$ electric double layer transistors. *Jpn. J. Appl. Phys.* **56**, 051101 (2017).
30. Imai, Y. *et al*. Superconductivity of $FeSe_{0.5}Te_{0.5}$ Thin Films Grown by Pulsed Laser Deposition. *Jpn. J. Appl. Phys.* **49**, 023101 (2010).
31. Imai, Y. *et al*. Systematic Comparison of Eight Substrates in the Growth of $FeSe_{0.5}Te_{0.5}$ Superconducting Thin Films. *Appl. Phys. Express* **3**, 043102 (2010).

Acknowledgements

This work was supported in part by JSPS KAKENHI (Grant Numbers 25708039 and 25220604) and CREST-JST.

Author Contributions

S.K., Y.K. and K.U. designed the research and analyzed the data. S.K. and Y.S. contributed to the device fabrication and the measurements of the transport properties and device characteristics. A.I. contributed to the TEM measurements. D.A., F.N., Y.I. and A.M. contributed to the film fabrication and to the XRD and AFM measurements. The text and figures of the paper were prepared by S.K., K.U. and A.M. All authors contributed to discussing the results reported in the manuscript.

Additional Information

Supplementary information accompanies this paper at https://doi.org/10.1038/s41598-018-33121-7.

Competing Interests: The authors declare no competing interests.

Publisher's note: Springer Nature remains neutral with regard to jurisdictional claims in published maps and institutional affiliations.

Open Access This article is licensed under a Creative Commons Attribution 4.0 International License, which permits use, sharing, adaptation, distribution and reproduction in any medium or format, as long as you give appropriate credit to the original author(s) and the source, provide a link to the Creative Commons license, and indicate if changes were made. The images or other third party material in this article are included in the article's Creative Commons license, unless indicated otherwise in a credit line to the material. If material is not included in the article's Creative Commons license and your intended use is not permitted by statutory regulation or exceeds the permitted use, you will need to obtain permission directly from the copyright holder. To view a copy of this license, visit http://creativecommons.org/licenses/by/4.0/.

© The Author(s) 2018